

# Synthesis, Characterization and Crystal Structure of New Organotin Copper Cyanide Three-Dimensional Supramolecular Coordination Polymer Containing Quinoxaline Molecule

Safaa Eldin H. Etaiw · Tarek A. Fayed ·  
Mohamed B. El-zaria · Safaa N. Abdou

Received: 30 June 2010/Accepted: 18 September 2010/Published online: 8 October 2010  
© Springer Science+Business Media, LLC 2010

**Abstract** Self assembly of  $K_3[Cu(CN)_4]$  with  $Me_3SnCl$  and quinoxaline (qox) affords the new organotin ternary adduct  $^3\infty[Cu_2(CN)_3 \cdot Me_3Sn \cdot qox]$ , **1**, as orange platelet crystals. The supramolecular architecture of **1** consists of  $[Cu_2(CN)_3]^-$  building blocks connected by the  $(Me_3Sn)^+$  cations forming infinite corrugated 1D-chains. The chains are bridged by the qox molecules forming 2D-layers containing fused distorted polygons. The layers are interwoven forming 3D-network structure, which are stabilized by close packing effects such as H-bonds as well as Cu···Cu and  $\pi$ - $\pi$  interactions. IR and mass spectra as well as TGA are investigated.

**Keywords** Supramolecular polymer · Organotin · Quinoxaline · Hydrogen bonds

## 1 Introduction

One of the most important characteristics of supramolecular organometallic compounds and coordination complexes, of course, is the structural variability. Several factors contribute to this structural variability, for example, the number and type of ligands and their combinations as well as the coordination geometry, the number of metal atoms and the presence of ionic charge [1]. Structural variability is intimately associated with other typical property of organometallic systems, namely structural flexibility. Thus, it is essential to take structural variability and flexibility into account when approaching

organometallic solids. It is well known that organometallic polymers possess unique properties and potential applications that are dependent on their organic segments and the types of metal complexes incorporated into their backbones or side chains [2]. In this aspect, the  $[Cu_n(CN)_m]_x$  building-block approaches are used here for the construction of multidimensional supramolecular coordination polymers by attempting to incorporate the  $(R_3Sn)^+$  cation as an essential element of the framework. This strategy allows for the synthesis of uncharged architectures in which channels remain, mostly, blocked by the R groups. A limited number of structural motifs is known for  $[Cu_m(CN)_n \cdot R_3Sn \cdot L]$  where L = bipodal organic ligand [3–7]. It is evident that none of these structures contain the quinoxaline moiety and the only free organotin example containing qox is  $[Cu_2(CN)_2 \cdot qox]$ , **1a** which exhibits 2D-framework [8]. Recently, a novel 3D-supramolecular coordination polymer (SCP) based on CuCN,  $Ph_3Sn$  cation and quinoxaline is reported [9].

In this paper the novel organotin-copper cyanide  $^3\infty[Cu_2(CN)_3 \mu-(Me_3Sn)\mu-(qox)]$  has been synthesized at room temperature and characterized by elemental analysis, IR, and mass spectra, TGA and single crystal X-ray diffraction.

## 2 Experimental

### 2.1 Materials and Physical Measurements

All preparative and analytical work was carried out under normal atmosphere. All the reagents for the synthesis were commercially available and employed without further purification.  $K_3[Cu(CN)_4]$  was prepared following the literature procedures [10, 11]. Elemental analysis was

S. E. H. Etaiw (✉) · T. A. Fayed · M. B. El-zaria · S. N. Abdou  
Chemistry Department, Faculty of Science, Tanta University,  
Tanta, Egypt  
e-mail: safaaetaiw@hotmail.com

performed on a Perkin-Elmer 2400 automatic elemental analyzer, while copper was determined using Perkin-Elmer 2380 atomic absorption spectrometer. Infrared spectra were recorded on a Bruker Vector 22 as KBr discs. X-ray diffraction was carried out on Kappa CCD Enraf-Nonius FR 590 four circle goniometer with graphite monochromatic MoK $\alpha$  radiation [0.71073 Å].

## 2.2 Synthesis of $^3\infty[\text{Cu}_2(\text{CN})_3 \cdot \text{Me}_3\text{Sn} \cdot \text{qox}]$ , 1

A solution of 90 mg (0.31 mmol) of  $\text{K}_3[\text{Cu}(\text{CN})_4]$  in 10 mL  $\text{H}_2\text{O}$  was added, under gentle stirring to a solution of 189 mg (0.95 mmol) of  $\text{Me}_3\text{SnCl}$  and 40 mg (0.31 mmol) of qox, in 20 mL of hot acetonitrile. After some days, orange platelet crystals started growing from the initially clear solution. After filtration, washing with small quantities of cold  $\text{H}_2\text{O}$  and acetonitrile and overnight drying, 81 mg (52.4% referred to  $\text{K}_3[\text{Cu}(\text{CN})_4]$ ) of the orange platelet crystals were obtained. Elemental analysis data for **1** ( $\text{C}_{14}\text{H}_{15}\text{N}_5\text{Cu}_2\text{Sn}$ ) are as follows, anal. Calcd: C, 33.68; H, 3.00; N, 14.03; Cu, 25.48. Found: C, 33.59; H, 3.09; N, 14.10; Cu, 25.40.

## 2.3 Single Crystal Structure Determination

The structure of **1** was solved using direct-methods and all of the non-hydrogen atoms were located from the initial solution or from subsequent electron density difference maps during the initial stages of the refinement. After locating all of the non-hydrogen atoms in each structure the models were refined against  $F^2$ , first using isotropic and finally anisotropic thermal displacement parameters. The positions of the hydrogen atoms were then calculated and refined isotropically and a final cycle of refinement was performed. Crystallographic data and structure refinement parameters of **1** are summarized in Table 1.

## 3 Results and Discussion

### 3.1 Crystal Structure of $^3\infty[\text{Cu}_2(\text{CN})_3 \cdot \text{Me}_3\text{Sn} \cdot \text{qox}]$ , 1

The ORTEP drawing of the asymmetric unit;  $^3\infty[\text{Cu}_2(\text{CN})_3 \cdot \text{Me}_3\text{Sn} \cdot \text{qox}] = ^3\infty[\{\text{Cu}(\text{CN})_2\mu-(\text{CN})\mu-(\text{Me}_3\text{Sn})\}\mu-(\text{qox})]$  of the SCP **1** indicates that **1** comprises of one qox molecule,  $[\text{Cu}_2(\text{CN})_3]$  fragment and one  $\text{Me}_3\text{Sn}$  cation (Fig. 1). The expanded structure shows that the  $[\text{Me}_3\text{Sn}]^+$  cations bridge the anionic  $[\text{Cu}_2(\text{CN})_3]^-$  building blocks forming infinite corrugated 1D-chains which are connected by the qox ligands creating 2D-layers (Fig. 2). Both Cu(I) sites assume distorted trigonal planer (TP-3) geometry through coordination to two cyanide groups and one qox ligand. In spite of the fact that the sum of the trigonal plane angles

**Table 1** Crystal data and structure refinement parameters of the SCP **1**

Empirical formula	$\text{C}_{14}\text{H}_{15}\text{N}_5\text{Cu}_2\text{Sn}$
Formula weight (g mol $^{-1}$ )	499.091
Temperature (K)	298
Wavelength (Å)	0.71073
Crystal system	Triclinic
Space group	$P\bar{1}$
$a$ (Å)	7.0462 (2)
$b$ (Å)	9.8461 (3)
$c$ (Å)	13.7973 (5)
$\alpha$ (°)	105.843 (2)
$\beta$ (°)	94.917 (4)
$\gamma$ (°)	108.076 (2)
$V$ (Å $^3$ ); $Z$	858.26 (5); 2
$D$ calc. (g cm $^{-3}$ )	1.931
$F(000)$	408
$\theta$ -range (°)	3.10–27.54
Reflections collected/unique	5484/2321
$R$ int	0.028
Data/restraints/parameters	2321/0/199
Goodness-of-fit on $F^2$	1.496
$R$ indices [ $I > 3\sigma(I)$ ] $R^1/\text{w}R^2$	0.033/0.061
$W = 1/s^2(F_0^2) + 0.1000 \times F_0^2$	
$R$ indices (all data)	0.075/0.074
Largest difference peak and hole (e Å $^{-3}$ )	0.92/-1.17

is  $\approx 360^\circ$ , qox causes distortion where the NC–Cu–qox angle is less than  $120^\circ$  due to weak but non negligible contact between Cu atom and C (qox) atom with a distance equals to 3.342 Å. It is indicated that Cu(2) site is more distorted than that of Cu(3) (Table 2). All the cyanide groups in the anionic  $[\text{Cu}_2(\text{CN})_3]^-$  building blocks are ordered, while the copper cyanide angles exhibit bent structure ( $165.02$ – $177.56^\circ$ ), Table 2.

The cyanide bond distance between Sn(I) and Cu(3) atoms is shorter (1.125 Å) than that of the other two cyanide groups (1.143 Å) while they all are shorter than those reported for the tin free prototype  $[\text{Cu}_2(\text{CN})_2(\text{qox})]$  [8], **1a**. The tin atom assumes TBPY-5 geometry where the three methyl groups orient themselves toward the corners of a distorted TP-3 with C–Sn–C angles equal to  $\approx 360^\circ$  (Table 2). The nitrogen atoms of the cyanide groups occupy axial positions which exhibit nearly right angles;  $89.98^\circ$ , with respect to the  $\text{Me}_3\text{Sn}$  plane (Table 2). However, the N(25)–Sn(I)–N(26) angle is  $173.31^\circ$  which reflects a bent structure of the (CN–Me<sub>3</sub>Sn–NC) connecting unit and the fact that the methyl groups occupy perpendicular positions out of the plane defined by CN–Sn–NC spacer. Thus, the  $[\text{Cu}_2(\text{CN})_3]^-$  building blocks and the  $[\text{Me}_3\text{Sn}]^+$  connecting units are the basic units

**Fig. 1** ORTEP drawing of the asymmetric unit of **1**, showing the atom labeling scheme and thermal ellipsoids are shown 50% probability

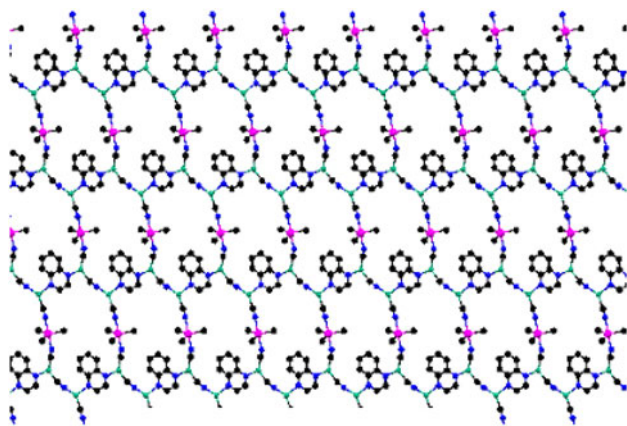
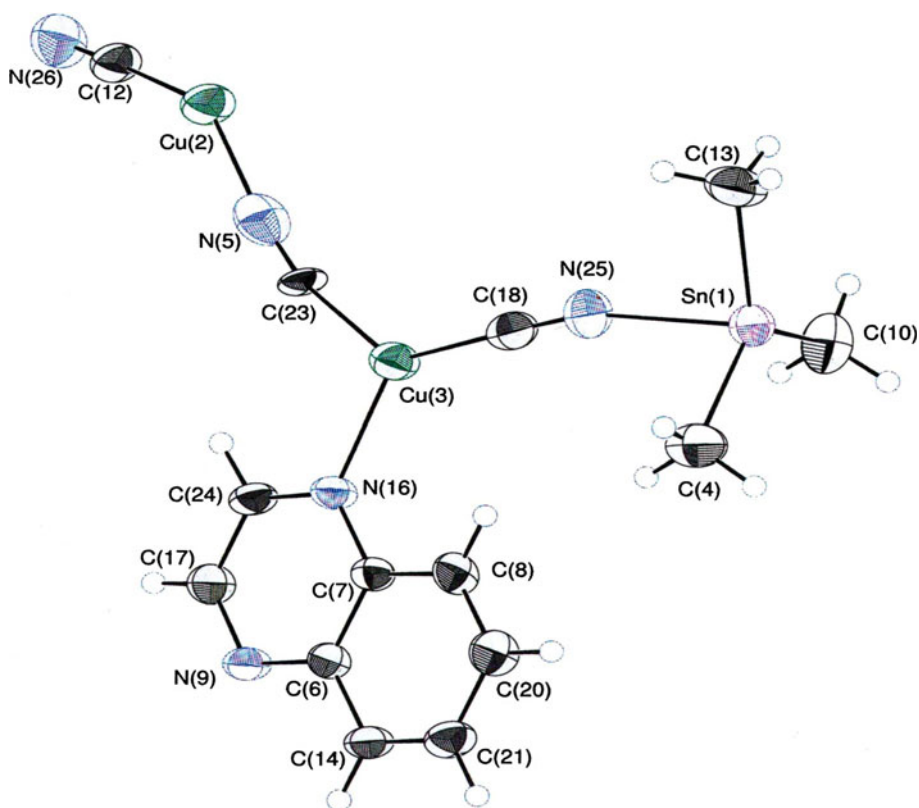


**Fig. 2** A view of the 2D-layer of the SCP **1** along the *a*-axis showing the distorted fused hexagonal  $[(\text{CuCN})_6(\text{Me}_3\text{Sn})_2(\text{qox})_2]$  rings. Hydrogen atoms are omitted for clarity

constructing the corrugated chains of **1** which are more puckered than the chains of **1a** due to the presence of the non linear CuCN and the CN–Sn–NC spacer as well as the distorted TP-3 Cu geometry. The distance between the corrugated chains is 9.846 Å. These parallel corrugated chains along the *a*-axis are bridged by the qox molecules forming 2D-layer structure via construction of fused

**Table 2** Selected bond lengths (Å) and bond angles (°) for the SCP **1**

Sn(l)–C(4)	2.109 (4)	C(4)–Sn(l)–C(13)	126.80 (13)
Sn(l)–C(10)	2.112 (3)	C(4)–Sn(l)–N(25)	87.72 (12)
Sn(l)–C(13)	2.125 (3)	C(4)–Sn(l)–N(26)	88.15 (12)
Sn(l)–N(25)	2.330 (3)	C(10)–Sn(l)–C(13)	155.71 (14)
Sn(l)–N(26)	2.344 (3)	C(10)–Sn(l)–N(25)	92.13 (11)
Cu(2)–N(5)	1.935 (3)	C(10)–Sn(l)–N(26)	94.44 (12)
Cu(2)–N(9)	2.183 (2)	C(13)–Sn(l)–N(25)	88.68 (12)
Cu(2)–C(12)	1.902 (3)	C(13)–Sn(l)–N(26)	89.58 (13)
Cu(3)–C(18)	1.894 (3)	N(25)–Sn(l)–N(26)	173.31 (10)
Cu(3)–N(16)	2.079 (2)	N(5)–Cu(2)–N(9)	112.72 (9)
Cu(3)–C(23)	1.902 (3)	N(5)–Cu(2)–C(12)	138.85 (10)
N(5)–C(23)	1.143 (4)	N(9)–Cu(2)–C(12)	108.39 (10)
C(6)–N(9)	1.378 (3)	Cu(2)–C(12)–N(26)	177.56 (3)
C(7)–N(16)	1.369 (3)	C(12)–Cu(2)–C(17)	84.81 (10)
N(9)–C(17)	1.316 (4)	N(16)–Cu(3)–C(18)	127.26 (11)
C(12)–N(26)	1.142 (4)	N(16)–Cu(3)–C(23)	103.42
N(16)–C(24)	1.317 (3)	C(18)–Cu(3)–C(23)	129.31 (12)
C(18)–N(25)	1.125 (4)	C(18)–Cu(3)–C(24)	150.73 (11)
C(4)–Sn(l)–C(10)	117.46 (13)	C(23)–Cu(3)–C(24)	79.96 (9)
Cu(3)–C(23)–N(5)	165.02 (2)	Cu(2)–N(5)–C(23)	172.3 (2)
Sn(l)–N(26)–C(12)	160.6 (3)	Cu(2)–N(9)–C(6)	128.2 (2)
Sn(l)–N(25)–C(18)	162.9 (2)	Cu(2)–N(9)–C(17)	114.8 (2)
Cu(3)–C(18)–N(25)	172.5 (3)		

distorted polygons of the composition  $\text{Cu}_6(\text{CN})_6(\text{Me}_3\text{Sn})_2(\text{qox})_2$  creating wide space enough to accommodate the qox and the methyl molecules (Fig. 2). These polygons have dimensions of  $9.846 \times 17.140 \text{ \AA}$ . The  $(\text{CuCN})_6(\text{Me}_3\text{Sn})_2(\text{qox})_2$  rings are bent and twisted to a certain degree. These distortions have been likened by Pretsch and Hartl [12] to these occurring in cyclohexane rings, for example chair and boat conformation. In the title compound, the  $(\text{CuCN})_6(\text{Me}_3\text{Sn})_2(\text{qox})_2$  rings all adopt a chair conformation.

The 2D-corrugated layers are arranged in a parallel way along the b-axis producing  $(\text{AB}\cdots\text{AB}\cdots\text{AB})_\infty$  unique system (Fig. 3). The infinite AB layers are interwoven along the a- and the c-axis where one qox molecule and the methyl groups in one layer fill the space of the polygon in another layer while the parallel qox rings avoid any  $\pi\cdots\pi$  interaction (Fig. 4). Alternatively, the AB layers form parallel channels along the b-axis with variable interlayer distances;  $3.124\text{--}7.016 \text{ \AA}$ , while the qox molecules and the methyl groups are oriented out of these channels as they are directed to the space of the channel between the  $\text{AB}\cdots\text{AB}\cdots\text{AB}$  layers (Fig. 3). On the other hand, the separation distance between the  $\text{AB}\cdots\text{AB}$  layers along the a-axis (i.e. between A $\cdots$ A or B $\cdots$ B) is  $7.046 \text{ \AA}$ . The 2D-layers of these distorted hexagonal nets, stacked in an  $\cdots\text{AB}\cdots\text{AB}\cdots$  fashion represent yet another variant of the honeycomb net observed previously in a number of  $[\text{ACu}_2(\text{CN})_3\cdot n\text{H}_2\text{O}]$  compounds, where A can be a single or complex cation [13]. The facing qox rings along the a- or the c-axis are quite parallel to each other in spite of the fact that the qox plane is rotated only a  $8.29^\circ$  out of the layer plane. The A $\cdots$ B layers adopt broad wave structure in which the methyl groups look like pillars oriented at the bottom of the waves between the  $\text{AB}\cdots\text{AB}\cdots\text{AB}$  layers. Thus, the methyl groups of the  $\text{Me}_3\text{Sn}$  units orient

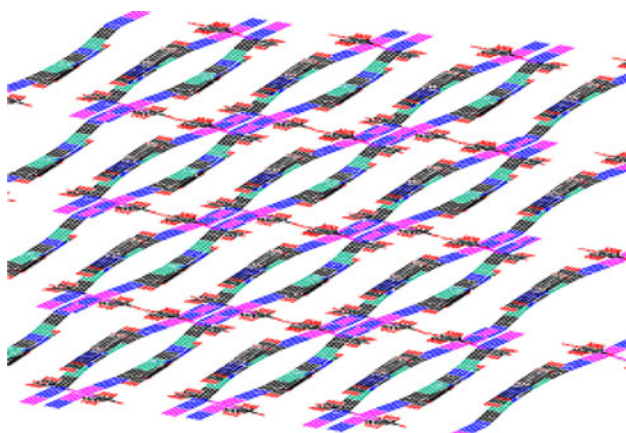


**Fig. 3** A view of the network structure of the SCP 1 along the b-axis showing the orientation of the qox ligand and the methyl groups between the layers

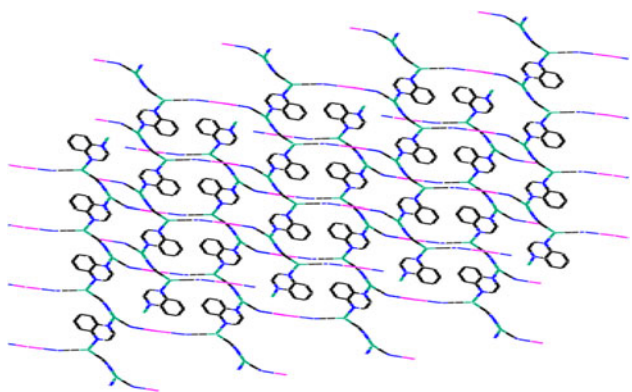


**Fig. 4** A view of the network structure of the SCP 1, showing the interwoven layers along the c-axis. Hydrogen atoms and methyl groups are omitted for clarity

**Table 3** Selected hydrogen bond lengths ( $\text{\AA}$ ), Cu–contacts and  $\pi\cdots\pi$  stacking interactions in the A $\cdots$ B layer

Cu(2)–H(14)	2.9837(3)	C(18)–H(8)	2.702(3)
Cu(2)–H(17)	2.9407(3)	C(23)–H(24)	2.604(2)
Cu(3)–H(8)	2.8446(4)	N(25)–H(4C)	2.858(3)
Cu(3)–H(24)	2.9220(3)	N(25)–H(13C)	2.869(3)
N(5)–H(10B)	2.987(2)	N(26)–H(13B)	2.900(3)
C(12)–H(17)	2.793(3)	N(26)–H(13A)	2.867(3)
C(13)–H(4A)	2.924(3)	Sn(1)–H(4A)	2.582
Sn(1)–H(4C)	2.602	Cu(2)–C(17)	2.984
Cu(2)–Cu(2)	7.016	C(6)–C(6)	3.540
Cu(3)–Cu(3)	3.124	Cu(2)–C(8)	3.330
C(12)–N(9)	3.317	N(26)–C(10)	3.274
C(18)–C(23)	3.346	Cu(3)–C(23)	3.149

themselves by unique way through the A $\cdots$ B layers to form H-bonds, Table 3. These extensive H-bonds are between H-atoms of the methyl groups and both the cyanide groups exhibiting a bond distance of  $2.858\text{--}2.987 \text{ \AA}$  and the Sn(I) atoms with a distance of  $2.582\text{--}2.602 \text{ \AA}$ . There are, also, extensive H-bonds in the A $\cdots$ B layers between H-atoms of qox molecules and the cyanide ligands as well as with Cu(2) and Cu(3) atoms in the range of  $2.703\text{--}2.9837 \text{ \AA}$ . The A $\cdots$ B layers are further stabilized by extensive  $\pi\cdots\pi$  stacking and short contacts between the cyanide ligands;  $3.346\text{--}3.587 \text{ \AA}$ , the cyanide ligand and the qox molecules;  $3.317\text{--}3.656 \text{ \AA}$ , the cyanide ligand and the methyl group;  $3.274 \text{ \AA}$ , the Cu(2) atoms and the qox molecules;  $2.984\text{--}3.342 \text{ \AA}$  and the Cu(3) atoms and the cyanide ligands;  $3.149 \text{ \AA}$ . On the other hand, extensive attention has been now focused on the fact that group II metals in the +1 oxidation state have a tendency to form clusters, often with quite short metal–metal bond lengths [14, 15]. The Cu(I)–Cu(I) closed-shell interactions (CSI) have been early

**Table 4** The  $\pi$ – $\pi$  stacking interaction, Cu-contacts, H-bonds and the separation distances ( $\text{\AA}$ ) between the AB…AB…AB layers

Cu(2)–C(14)	3.309	C(6)–N(5)	3.321
Cu(2)–C(21)	3.321	N(9)–H(14)	3.105
Cu(3)–C(17)	3.629	C(13)–H(13C)	3.134
C(17)–C(23)	3.683	C(13)–H(4A)	2.925
C(14)–N(9)	3.519	C(4)–H(13C)	3.290
N(9)–N(5)	3.747		

supported by extended Hückel calculations proposed hybridization effects between filled ( $n-1$ )  $d$ -orbitals and the ns and np orbitals [16–18]. The term “cuprophilicity” has been coined to describe the Cu(I)–Cu(I) bonding interaction [19]. Recently, there are evidences that the oligomerization of the dimmers  $[\text{M}_2\text{L}_2]$  is favored by stronger metallophilic and weaker face-to-face  $\pi$ – $\pi$  interactions where M is Cu(I) or Ag(I) [20]. In **1**, the A…B layers exhibit crystal packing effects due to Cu(3)–Cu(3) interaction; 3.124  $\text{\AA}$ . The shortest distance of Cu(2)–Cu(2) is 7.016  $\text{\AA}$  avoiding any Cu(2)–Cu(2) interactions. Also, the AB…AB…AB layers are stabilized by close packing effects such as H-bonds; 2.925–3.290  $\text{\AA}$ ,  $\pi$ – $\pi$  stacking (3.371–3.727  $\text{\AA}$ ) and the Cu contacts (3.309–3.629  $\text{\AA}$ ) (Table 4). The shortest Cu–Cu distances in the AB…AB…AB layers are Cu(2)–Cu(2) = 5.409  $\text{\AA}$  and Cu(3)–Cu(3) = 12.479  $\text{\AA}$  while the separation distance between tin atoms is 17.574  $\text{\AA}$ .

For comparison, the structure of **1** is quite different from that of  $[\text{Cu}(\mu\text{-pyz})\{\mu\text{-CNSn}(\text{Me}_3)\text{NC}\}]$ , pyz = pyrazine; **1b** [4], in spite of the fact that both the uncharged bipodal ligands, pyz and qox and the likewise rodlike anionic  $\{\text{CN}-\text{Sn}(\text{Me}_3)\text{NC}\}$  unit may act as nanometer-sized spacer in both compounds. The structure of **1** is based on infinite non linear chains that contain the distorted TP-3 Cu(I) sites and the TBPY-5 configured Sn sites creating layers containing fused non interpenetrating distorted polygons. However, the asymmetric unit of **1b** is surprisingly simple containing one Cu(I) atom, one cyanide group which connects the Cu(I) atoms and  $\text{Me}_3\text{Sn}$  group, and one pyz ring [4]. **1** contains also the anionic  $[\text{Cu}_2(\text{CN})_3]^-$  building blocks which are connected by the  $\text{Me}_3\text{Sn}$  units forming corrugated chains which are connected by the qox rings forming the 3D interwoven layered structure. Distorted-adamondoid Cu(10) cages whose surfaces are surrounded either by  $\text{Cu}_6(\text{pyz})_4\{\text{Sn}-(\text{NC})_2\}_2$  or by  $\text{Cu}_6(\text{pyz})_2\{\text{Sn}-(\text{NC})_2\}_4$  rings are observed in the 3D-frameworks of **1b**. Because of the large internal voids within each of Cu(10) cages, three equivalent frameworks are found interpenetrating each other. The Cu(2)–N(9)(qox) distance of **1** exceed those found in **1b** [4] and in other pyrazine complexes of Cu(I) [21] while Cu(3)–N(16)(qox) distance is shorter than

them. Thus, the Cu(2)–qox–Cu(3) distance of 7.096  $\text{\AA}$  is shorter than that in **1b** which equals almost the Ag–pyz–Ag distance 7.225  $\text{\AA}$  reported for  $[\text{Ag}(\text{pyz})\text{NO}_3]$  [22]. Also, the structure of **1** is quite different from that of the  $\text{Me}_3\text{Sn}$  free  $[\text{Cu}_2(\text{CN})_2(\text{qox})]$ , **1a**. The network of **1a** is constructed of  $\{\text{CuCN}\}_\infty$  chains linked through qox ligands into a two-dimensional sheet. The structure adopts non-interpenetrating  $\{\text{Cu}_6(\text{CN})_4(\text{qox})_2\}$  rings [8]. Interestingly, again the structure of **1** differs, however, once more from the structures of  $[\text{Cu}_2(\text{CN})_4(\text{Ph}_3\text{Sn})_2\cdot\text{qox}]$ , **1c**, [9],  $[\text{Cu}(\text{CN})_2\cdot\text{Me}_3\text{Sn}\cdot 0.5 \text{ bpy}]$ , **1d**, [3],  $[\text{Cu}(\text{CN})_2\text{Me}_3\text{Sn}\cdot 0.5 \text{ bpe}]$ , **1e**, [5],  $[\text{Cu}(\text{CN})_2\text{Me}_3\text{Sn}\cdot 0.5 \text{ bpeH}_2]$ , **1f**, [5] and  $[\text{Cu}(\text{CN})_2\text{Me}_3\text{Sn}\cdot\text{cpy}]$ , **1g**, [5] where bpy = 4,4'-bipyridine, bpe = bis(4-pyridyl)-*trans*-ethene, 0.5 bpeH<sub>2</sub> = bis(4-pyridyl)-1,2-ethane and cpy = 4-cyanopyridine. Surprisingly, in spite of the fact that **1d–g** have the same chemical composition  $[\text{Cu}(\text{CN})_2\text{Me}_3\text{Sn}.\text{L}]$ , they exhibit diverse topologies depending on the type of the ligand L.

### 3.2 Infrared and Mass Spectra of **1**

The IR spectrum of **1** exhibits the characteristic bands of the ternary adducts  $\text{Me}_3\text{Sn}$  units, cyanide group and the qox molecule (Table 5). The band at 2119  $\text{cm}^{-1}$  can be considered as a good evidence of the formation of non-linear chains of the  $[-\text{Cu}-\text{C}\equiv\text{N}-\text{Me}_3\text{Sn}-\text{N}\equiv\text{C}-\text{Cu}-]$  fragment [23, 24]. However, the band at 2070  $\text{cm}^{-1}$  indicates the presence of another kind of the cyanide ligand in the structure of **1** which may be coordinated to two copper atoms. This opinion is further supported by the appearance of the medium band due to stretching vibrations of the Cu–C bond as doublet at 411 and 407  $\text{cm}^{-1}$ . The presence of the  $\text{Me}_3\text{Sn}$  units is supported by the bands at 2917  $\text{cm}^{-1}$  ( $\nu_{\text{asym C-H}}$ ) and 2850  $\text{cm}^{-1}$  ( $\nu_{\text{sym C-H}}$ ) of the methyl groups. The  $\nu_{\text{Sn-C}}$  bond exhibits sharp band at 551  $\text{cm}^{-1}$  which reflects the presence of TBPY-5 configured  $\text{Me}_3\text{SnN}_2$  units in the network of **1**. The position as well as the relative weak intensity of the bands at 1585 and 1579  $\text{cm}^{-1}$  ( $\nu_{\text{C=C}}$ ) reflect the participation of the nitrogen atoms of the qox ligand in coordination with the copper atoms.

The constitution of the SCP **1** is also established by mass spectrometry (Table 6). The mass spectrum of **1** exhibits the base peak at  $m/z$  130 corresponding to the molecular ion of qox. Also, the mass spectrum displays the ion peaks at  $m/z$  = 126 and 191 corresponding to  $\text{Me}_2\text{SnCN}^+$  and  $\text{Me}_3\text{SnCN}^+$ , respectively. In addition, the mass spectrum shows the ion peaks at  $m/z$  = 250, 306, 367 and 433 due to  $[\text{Cu}(\text{CN})_2\text{MeSn}]^+$ ,  $[\text{Cu}_2\text{CNMe}_2\text{Sn}]^+$ ,  $[\text{Cu}_2(\text{CN})_3\text{Me}_3\text{Sn}]^+$ ,  $[\text{Cu}_2\text{CNMe}_2\text{Sn}(\text{qox})]^+$ , respectively. Thus, the mass spectrum indicates that **1** contains the qox,  $\text{Me}_3\text{Sn}$  and CuCN fragments.

**Table 5** Wavenumbers ( $\text{cm}^{-1}$ ) of the different vibrational modes of the SCP **1**

Band	Assignment	Band	Assignment	Band	Assignment
3093 w	$\nu_{\text{CH}}$ (a)	1585 w	$\nu_{\text{C}=\text{N}}$	1136 s	Vibrations of qox ring
3065 w				1090 w	
3006 m				1047 s	
				964 s	
2917 m	$\nu_{\text{CH}}$ (m)	1579 w	$\nu_{\text{C}=\text{C}}$	863 m	$\gamma_{\text{CH}}$
2850 w		1544 sh		783 (m)	
		1501 s			763 s
2119 s	$\nu_{\text{C}\equiv\text{N}}$	1462 m (m)	$\delta_{\text{CH}}$	551 s	$\nu_{\text{Sn}-\text{C}}$
2070 sh		1407 sh			
		1376 m (m)			
1951 w	Overtones and combinations of the phenyl rings	1358 s		411 m	$\nu_{\text{Cu}-\text{C}}$
1833 w		1209 s	$\nu_{\text{C}-\text{N}}$	407 m	
1750 w					
1721 w					

a aromatic, (m) methyl, s strong, sh shoulder, m medium, w weak

**Table 6** The mass spectral data of the of  ${}^3_{\infty}[\text{Cu}_2(\text{CN})_3 \cdot \text{Me}_3\text{Sn-qox}]$ , **1**

Assignment	$m/z$	Assignment	$m/z$
$\text{C}_2\text{H}_2^+$	26	$\text{Me}_3\text{Sn}^+$	165
$\text{C}_4\text{H}_2^+$	50	$\text{Me}_2\text{SnCN}^+$	176
$\text{C}_6\text{H}_4$	76	$\text{Me}_3\text{SnCN}^+$	191
$\text{C}_7\text{H}_5\text{N}^+$	103	$[\text{Cu}(\text{CN})_2\text{MeSn}]^+$	250
$\text{Sn}^+$	120	$[\text{Cu}_2\text{CNMe}_2\text{Sn}]^+$	306
$[\text{qox}]^+$	130	$[\text{Cu}_2(\text{CN})_3\text{Me}_3\text{Sn}]^+$	367
$\text{MeSn}^+$	135	$[\text{Cu}_2\text{CNMe}_2\text{Sn}(\text{qox})]^+$	433
$\text{Me}_2\text{Sn}^+$	150	–	–

### 3.3 Thermogravimetric Analysis of **1**

The SCP **1** undergoes thermolysis in four steps (Table 7). The first step is in the temperature range 110–200 °C and it is due to the decomposition of the more volatile connecting unit  $\text{Me}_3\text{Sn}$ . This step is followed by the loss of qox molecule in the temperature range 210–370 °C. The

third step corresponds to the loss of one cyanide group in the temperature range 380–450 °C. These steps are followed by an increase in mass due to the gain of the mass of an oxygen atom in the temperature range 460–560 °C. At higher temperatures (over 600 °C) the remaining cyanide groups are released, since **1** undergoes complete decomposition to give the final product of cuprite and carbon.

### 4 Discussion

The self assembling of  $[\text{Cu}_m(\text{CN})_n]^{x-}$  anions,  $\text{R}_3\text{Sn}^+$  cations and bipodal ligand (L) to form such 3D-polymers, **1** and **1b–g**, is the quintessence of the self-recognition and self aggregation processes which are supramolecular chemistry paradigms. In spite of they are formed using the same reactants, they exhibit diverse topologies containing different building blocks;  $[\text{Cu}_2(\text{CN})_3]^-$ ,  $[(\text{Cu}(\text{CN})_2)^-]$  and  $[(\text{Cu}_2(\text{CN})_4)^{2-}]$ . It is worth mentioning that none of the structures of these SCP contain the  $[\text{Cu}(\text{CN})_4]^{3-}$  anion

**Table 7** Thermogravimetric analysis data of the SCP **1**

Temp. range (°C)	$\Delta m_{\text{obs}}\%$ mass unit (M.W.) ( $\text{g mol}^{-1}$ )	$\Delta m_{\text{cal}}\%$ mass unit (M.W.) ( $\text{g mol}^{-1}$ )	Steps
110–200	–33.03% (164.75)	–32.81% (163.7)	$-[\text{Me}_3\text{Sn}]$
210–370	–26.42% (131.80)	–26.06% (130)	$-[\text{qox}]$
380–450	–5.36% (26.77)	–5.21% (26)	$-(\text{CN})$
460–560	+3.30% (16.47)	+3.20% (16)	$+[\text{O}]$
Over 600	38.49% (191.98)	38.31% (191.1)	$\text{Cu}_2\text{O} + 4\text{C}$

which is one of the starting materials. It seems that  $\text{Me}_3\text{SnCl}$  or  $\text{Ph}_3\text{SnCl}$  may cause decomposition of the tetrahedral  $[\text{Cu}(\text{CN})_4]^{3-}$  anion to different  $[\text{Cu}_m(\text{CN})_n]^{x-}$  fragments, which are readily assembled with the other reactants in solution to produce the thermodynamically more stable SCP. The presence of  $\text{R}_3\text{SnCl}$  seems to be essential for the reaction to proceed thermodynamically at room temperature, the point which needs further investigation. However, it is known that the  $\text{Me}_3\text{SnCl}$  molecule has weak Sn–Cl bond, as the non polar trimethyl tin units are bridged to the chlorine atoms by unequal, relatively large, (2.470 and 3.269 Å) distances [25]. The  $\text{Me}_3\text{SnCl}$  may form, in this case, the more stable  $\text{Me}_3\text{SnCN}$ , as the Sn–C or the Sn–N bond distances of the ordered C–N–Sn–N–C or even N–C–Sn–C–N chains are in the range of  $2.49 \pm 0.02$  Å or may form the  $(\text{Me}_3\text{Sn})_2$  dimer [26, 27]. Consulting the structures of these SCP, it is evident that the shape and size of the ligand play an essential role for creating such diverse topologies. The copper coordination geometry and the orientation of the interaction sites in the ligand provide the instructions for the self-assembly of the proposed supramolecular assembly. A current research work indicates that these organotin SCP, specially **1** and **1c**, have been shown to be cytotoxic to human tumor cells. Also, these SCP should have potential applications in areas such as catalysis and photoluminescence, which are the subject of future research work.

#### 4.1 Supplementary Data

CCDC 737371 contains the supplementary crystallographic data for **1**. These data can be obtained free of charge via <http://www.ccdc.cam.ac.uk/conts/retrieving.html>, or from the Cambridge Crystallographic Data Center, 12 Union Road, Cambridge CB2 1EZ, UK; fax: (+44) 1223 336 033; or e-mail: deposit@ccdc.cam.ac.uk.

#### References

- D. Braga, F. Grepioni, Chem. Commun. 571(1996)
- A.S. Abd-El-Aziz, P.O. Shipman, B.N. Boden, W.S. McNeil, Prog. Polym. Sci. **35**, 714 (2010) and references therein
- A.M.A. Ibrahim, E. Siebel, R.D. Fischer, Inorg. Chem. **37**, 3521 (1998)
- E. Siebel, A.M.A. Ibrahim, R.D. Fischer, Inorg. Chem. **38**, 2530 (1999)
- H. Hanika-Heidl, S.E.H. Etaiw, M.Sh. Ibrahim, A.S. Badr El-din, R.D. Fischer, J. Organomet. Chem. **684**, 329 (2003)
- S.E.H. Etaiw, T.A. Fayed, S.N. Abdou, J. Organomet. Chem. **695**, 1918 (2010)
- S.E.H. Etaiw, T.A. Fayed, S.N. Abdou, J. Inorg. Organomet. Polym. **20**, 326 (2010)
- D. J. Chesnut, D. Plewak, J. Zubieta, J. Chem. Soc. Dalton Trans. 2567(2001)
- S. E. H. Etaiw, S. N. Abdou, J. Inorg. Organomet. Polym. (2010). doi:[10.1007/s10904-010-9383-4](https://doi.org/10.1007/s10904-010-9383-4)
- J.W. Eastes, W.M. Burgess, J. Am. Chem. Soc. **64**, 1187 (1942)
- J.W. Eastes, W.M. Burgess, J. Am. Chem. Soc. **64**, 2715 (1942)
- T. Pretsch, H. Hartl, Z. Anorg. Allg. Chem. **630**, 1581 (2004)
- A.H. Pohl, A.M. Chippindale, S.J. Hibble, Solid State Sci. **8**, 379–387 (2006)
- M. Janson, Angew. Chem. **99**, 1136 (1987)
- M. Janson, Angew. Chem. Int. Ed. Engl. **26**, 1043 (1987)
- K. Mchrotra, R. Hoffmann, Inorg. Chem. **17**, 2187 (1978)
- R. Hoffmann, A. Dedieu, J. Am. Chem. Soc. **100**, 2074 (1978)
- Y. Jiang, S. Alvarez, R. Hoffmann, Inorg. Chem. **24**, 749 (1985)
- J. M. Goodwin, P.-C. Chiang, M. Brynda, K. Penkina, M. M. Olmstead, T. E. Patten, Dalton. Trans. 3086–3092(2007)
- J.-P. Zhang, Y.-B. Wang, X.-C. Huang, Y.-Y. lin, X.-M. Chen, Chem. Eur. J. **11**, 552 (2005)
- S. Kitagawa, M. Munakata, T. Tanimura, Inorg. Chem. **9**, 1714 (1997)
- R.G. Vramka, E.L. Amma, Inorg. Chem. **5**, 1020 (1966)
- A.M.A. Ibrahim, J. Organomet. Chem. **556**, 1–9 (1998)
- P. Apodaca, F.C. Lee, H.K. Pannell, Main Group Met. Chem. **24**, 597 (2001)
- J.L. Lefferts, K.C. Molly, M.B. Hossain, D. Vander Helen, J.J. Zucker-man, J. Organomet. Chem. **240**, 349 (1982)
- P. Avalle, R.K. Harris, H. Hanika-Hiedle, R.D. Fischer, Solid State Sci. **6**, 1069 (2004)
- S.E.H. Etaiw, S.A. Amer, M.M. El-bendary, Polyhedron **28**, 2385 (2009)